Remotely Actuated Optothermal Robotic Microjoints Based on Spiral Bimaterial Design

Belal Ahmad, Antoine Barbot, Gwenn Ulliac, Aude Bolopion

Remotely Actuated Optothermal Robotic Microjoints Based on Spiral Bimaterial Design

Belal Ahmad, *Member*, *IEEE*, Antoine Barbot, Gwenn Ulliac, and Aude Bolopion, *Member*, *IEEE*

In this article, we propose laser actuated microjoints which can be remotely actuated in both air and water. Their actuation relies on the optothermal response of a spiral bimaterial. The microjoints are fabricated using two-photon polymerization technology that offers the ability to tune the thermal and mechanical properties of the material by controlling the laser printing power. Modeling is first conducted to verify the parameters of the spiral that affect the rotational displacement and generated torque of the microjoint. Then, microjoints having a diameter of less than 200 µm are characterized. The microjoints can realize a maximum deflection of approximately 8.5°, a force in the µN-order using a 265-µm long arm, an actuation repeatability of more than 100 times, and a time response of approximately 34 ms. Finally, the microjoints are implemented in a microgripper and an xy serial microarm. Successful micromanipulation of 40 µm microbeads using the microgripper, and the simultaneous actuation of multiple microjoints of the xy serial microarm with two degrees of freedom are shown. This kind of rotational, compact, selective, and remotely actuated microjoints would allow the deployment of individually controlled mobile microrobots with several degrees of freedom for complex applications such as cell manipulation and microassembly.

***Index Terms*—Micro/nano robots, rotational microjoints, optothermal actuation, spiral bimaterials.**

I. Introduction

MICROROBOTS have significantly evolved and attracted more attention in the past three decades due to the large advancement in microfabrication, microscopy, and microimaging technologies. They could revolutionize highly demanding domains including microassembly and biomedical applications [1], [2]. Nonetheless, microrobots are still a long way behind their macroscale counterparts mainly due to the lack of active joints, which are one of the main building blocks of conventional robots. This limitation mainly arises from the difficulty in fabricating, integrating, and controlling active elements, such as linear and rotational motors, at the meso and microscale. Moreover, in the case of mobile microrobots, the difficulty of adding active elements is increased due to the untethered nature of the microrobot requiring a wireless power transmission scheme [3].

A number of microactuators have been developed and utilized as active joints to actuate legged microrobots and microgrippers. They are based on magnetic [4], [5], pH [6], thermal [7], electrical [8], and optical [9]. For instance, pH controlled bimaterial microjoints have been developed to actuate a legged soft microrobot with non-identical swelling bilayers [6]. However, this approach

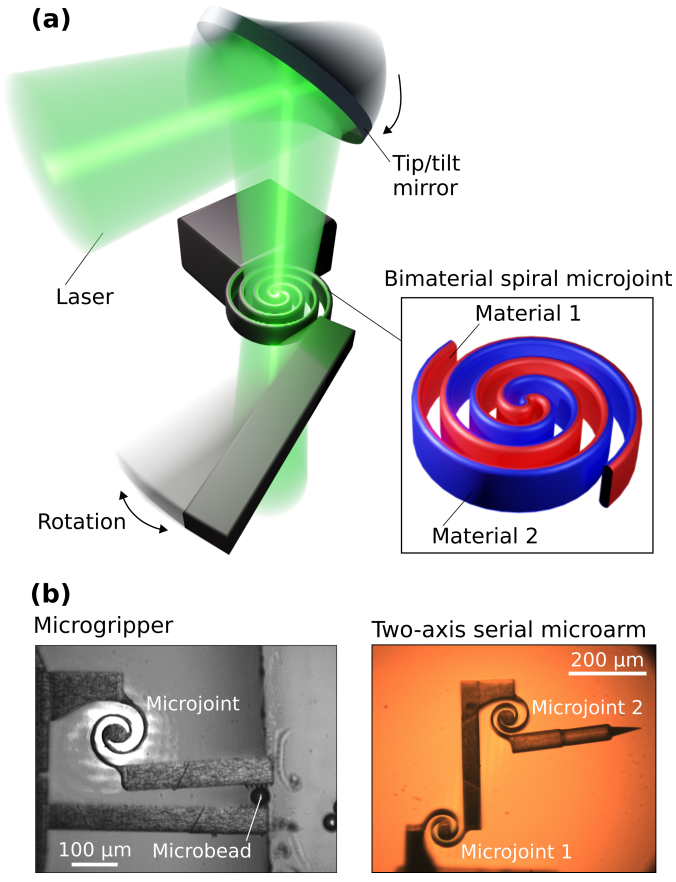

Fig. 1. (a) Conceptual image of the proposed bimaterial spiral microjoints demonstrating a rotational displacement when heated by a laser beam. (b) Microrobotic applications of the spiral microjoints.

Manuscript received September 29, 2021; revised December 21, 2021; accepted January 16, 2022. This paper was recommended for publication by Senior Editor W.J. Chris Zhang upon evaluation of the reviewers' comments. This work was supported in part by the EIPHI Graduate School under Contract ANR-17-EURE-0002, in part by the MiMedi project funded by BPI France under Grant DOS0060162/00 and the European Union through the European Regional Development Fund of the Region Bourgogne-Franche-Comté under Grant FC0013440, in part by the French ROBOTEX network and its Micro and Nanorobotics center under Grant ANR-10-EQPX-44-01 and in part by the french RENATECH network and its FEMTO-ST technological facility.

B. Ahmad, A. Barbot, G. Ulliac, and A. Bolopion are with FEMTO-ST Institute, Univ. Bourgogne Franche-Comté, CNRS, Besançon, France (e-mail: antoine.barbot@femto-st.fr, gwenn.ulliac@femto-st.fr, aude.bolopion@femto-st.fr). Corresponding author: B. Ahmad (email: belal.ahmad@femto-st.fr).

can only be used in liquid mediums and the non-local nature of the pH stimuli introduces challenges in addressing individual microjoints. Thermal actuation that exploits the deformation of matter in response to the change in its temperature is one of the dominant approaches generating large displacements (Fig. 1). Among thermal actuation schemes, electrothermal actuation based on joule heating effect is widely used, where a layer of conductive material is incorporated [10]. Although these microactuators can generate relatively large displacements with fast response time, they lack compactness, i.e. generated displacement to microactuator size ratio, and are not suitable for mobile applications due to their tethered nature. Optothermal actuation utilizes light to generate heat at a specific location. Although it falls short in terms of the generated force and the ability to penetrate highly nontransparent media, it offers a highly promising alternative due to its localized nature, wireless energy transmission, and the relative simplicity in controlling the light path [11]. The selective and untethered nature of optothermal actuation makes it the best candidate to allow several degrees of freedom in one or multiple microrobots, and to develop mobile applications in both air or liquid mediums.

In general, optothermal microactuators are mainly implemented in bentbeam [12], [13], hot–cold arm [14], or bimaterial [15] designs. For instance, Elbuken et al. [12] have developed a photothermally actuated microgripper fabricated with a single polymeric layer (SU-8) and based on the bentbeam microactuator. The microgripper could be actuated in air medium remotely to realize an opening of 16 µm using a focused laser beam to heat up a connection spot between two arms of the bentbeam. Nonetheless, the bentbeam design depends heavily on the length of its arms drastically reducing the overall compactness. Furthermore, only the connection area between the arms is heated and the expansion in the arms relies solely on heat conduction imposing high actuation difficulty inside mediums with relatively large heat conductivity due to heat dissipation. Microactuators based on the hot–cold arm design also suffers from similar limitations and challenges mainly due to the use of long arm structures. On the other hand, the optothermal response can be enhanced by using thermoresponsive hydrogels [16], [17], such as PNIPAM, allowing a high thermal expansion, although this comes at the cost of considerably reducing the stiffness and the generated force. Despite the advantages of bimaterial-based optothermal microjoints, this area of research is still largely unexplored [18]. Bimaterials offer the merits of compact design, and relatively large angular displacements, making it a suitable candidate for realizing a rotational microjoint. However, previous designs of bimaterials at the microscale were mainly fabricated in long stripes, reducing their compactness and angular displacement.

In order to deform the overall beam actuator with a local compact heating, we propose in this article a spiral optothermal rotational microjoint that can be actuated in both air and liquid, as shown in Fig. 1. For this, we utilize a polymer fabricated using two-photon polymerization (2PP) fabrication method, which offers the ability to manipulate the thermal and mechanical parameters of the printed material by changing the printing laser power [15]. The spiral microjoint is selectively actuated by applying a focused laser beam to initiate a relatively large rotational displacement, which allows untethered actuation and the integration of multiple active joints in a microrobot. Moreover, the compact nature of the spiral design allows the utilization of a long strip of a bimaterial in a small area, where the whole actuator is actively heated, compensating for the heat dissipation, especially in liquid mediums. These advantages can bring micromechatronics and microrobots one-step closer to their macroscale counterparts by introducing controllable multi degrees of freedom (DOF) to performer dexterous tasks. The proposed microjoint can be utilized as building block to enable novel micromechatronic and microrobotic applications where simultaneous and remote actuation of multiple controllable joints is required. To our knowledge, there has been no work on developing a selectively actuated rotational microjoint based on optothermal actuation.

II. Microjoint Modeling

A bimaterial beam deflects in a specific direction when heated due to the different thermal expansion coefficients of the two materials, as shown in Fig. 2(a). In fact, choosing the appropriate parameters for a 2PP-printed bimaterial spiral structure is critical to realize a functional microjoint. The parametric design of the spiral structure is based on the Archimedes' spiral as shown in Fig. 2(b). The points on the spiral can be expressed in the Cartesian coordinates as:

$$x_s = (d_0 + \frac{p}{2\pi}\phi)cos(\phi) \tag{1}$$

$$y_s = (d_0 + \frac{p}{2\pi}\phi)sin(\phi) \tag{2}$$

where d_0 is the initial diameter of the spiral, p is the pitch (i.e. the distance between consecutive turns), and ϕ is the angular position with respect to the x-axis. The angular position (ϕ) can have values in the interval $[0, +\infty]$ and any value beyond 2π will increase the number of turns (n) beyond one turn. A rotational displacement can be realized upon heating by constructing a spiral with two materials having different thermal expansion coefficients and Young's modulus. In fact, the thermal response of bimaterial, specifically bimetalic, spirals has been widely utilized in thermostats for temperature measurement [19]. By fixing the inner end of the spiral, a rotational displacement at the outer end can be realized upon heating, as shown in Fig. 2(c). In addition, clockwise or counterclockwise displacements can be achieved by exchanging the positions of the two materials in the spiral structure. To minimize defects

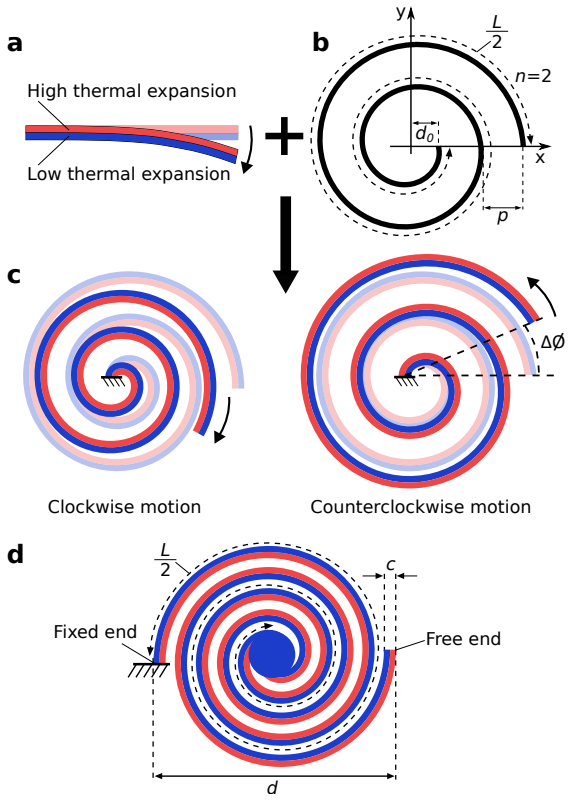

Fig. 2. Spiral microjoint modeling. (a) Deflection of a bimaterial beam in response to heat. (b) Archimedes' spiral and its parameters in the Cartesian coordinates. (c) Rotational displacement of bimaterial spirals and the effect of the materials position on the direction. (d) Bimaterial double-spiral having two connectable ends. The double-spiral parameters, mainly thickness (c), diameter (d), and half-length ($\frac{L}{2}$), are also shown on the figure.

and fabrication complexity, a 2.5-D design is chosen. Therefore, a double-spiral architecture is adapted by adding another spiral that is a shifted and mirrored version of the original spiral, where the two inner ends of the spirals are connected, as shown in Fig. 2(d). As a result, the double-spiral includes two outer ends that can be connected to the adjacent structures to function as a microjoint.

The rotational displacement produced in the bimaterial spiral in response to the temperature change is well approximated for small angular displacements (in radians) by [20]:

$$\Delta\phi = 2a\Delta T\frac{L}{c} \tag{3}$$

where L is the length of the spiral, c is the thickness of the spiral, $\Delta T = T - T_0$ is the temperature change from the initial (T_0) to the final (T) temperature, and a is the specific deflection of the bimaterial given as:

$$a = \frac{3}{4}(\alpha_2 - \alpha_1) \tag{4}$$

where α_1, α_2 are the thermal expansion coefficients of the two materials constituting the spiral. Eq. (3) holds true assuming that the translational deflection at the end of the spiral beam is smaller than 10% of its length L. It is worth mentioning that in this work the bimaterial is symmetric, i.e., the thickness is equal for both materials comprising the bimaterial ($c_1 = c_2 = c/2$). On the other hand, it is clear from eq. (3) that the spiral deflection is proportional to its length L, and inversely proportional to its thickness (c). Therefore, to realize large displacements, one can be tempted to maximize L and minimize c as much as possible. However, the torque generated by the microjoint is also largely affected by c, where a torque as high as possible is preferable to allow the implementation of the microjoint in applications requiring a high torque. The generated torque can be given as [20]:

$$\tau = k\Delta\phi \tag{5}$$

$$k = k_1 + k_2 = \frac{(E_1 + E_2)(I_1 + I_2)}{L} = \frac{(E_1 + E_2)hc^3}{48L} \tag{6}$$

where k_1, k_2, k are the stiffness constants of the first, second, and total spirals respectively, E_1, E_2, I_1, I_2 are the Young's moduli and the area moments of inertia of the first and second spirals respectively, and h is the vertical (z-axis) height of the spiral. Consequently, τ is proportional to the square of c. Therefore, the choice of the spiral parameters, mainly the thickness, should take in mind the trade-off between the required maximum rotational displacement and the required maximum torque to achieve a specific task. In addition, the length (L) would affect the diameter of the microjoint (d), where a minimal diameter is preferable to achieve a compact design, and to fully illuminate the microjoint with the laser spot for active heating, which is critical in case of in-liquid actuation.

III. Microjoint Characterization

A. Design, Fabrication, and Thermal Response

Microjoints for characterization purpose were designed and fabricated. The microjoints were connected to a fixed base structure from one end, and to a free arm structure from the other end. The arm structure acted as an indicator to quantify the rotational displacement of the microjoint when shined by the laser beam. The thickness of the whole structure including the spiral microjoint was h =50 µm. The diameter of the microjoint was chosen at d =130 µm to have a size that is as close as possible to the laser spot, while ensuring a well defined structure without unwanted material between the turns of the spiral that can arise from limitations in the fabrication process. The above dimensions will be used throughout the paper unless mentioned otherwise.

The spiral microjoint was fabricated by 2PP with Nanoscribe (Nanoscribe GmbH) using IP-S resin. The two materials in the spiral were achieved by using two different laser printing powers of 60% and 100% for the materials with high and low thermal expansion coefficient, respectively. By virtue of a printing accuracy

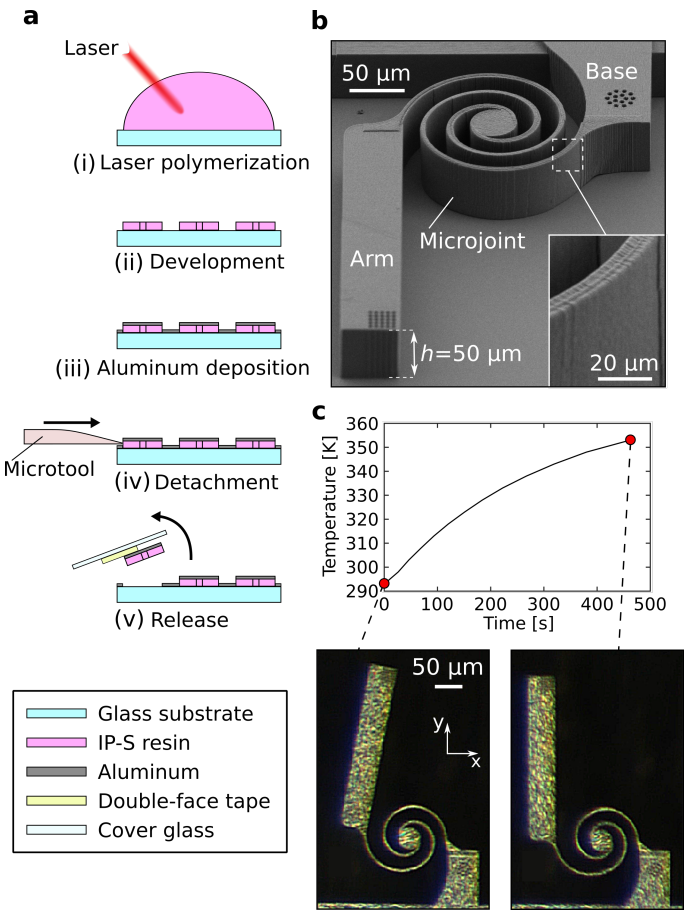

Fig. 3. (a) Fabrication process of the microjoint. (i) Laser polymerization of IP-S resin using 2PP. (ii) Development of the printed structures using PGMEA developer. (iii) Deposition of 600-nm thick aluminum layer. (iv) Detaching the structures using a manually operated microtool. (v) Release of the final structures using double-face adhesive tape. (b) SEM image of a fabricated microjoint with indication to the components and their height (h). (c) Experimental images showing the thermal response of a microjoint placed on a hot plate. The curve shows the increase of the hot plate temperature with time.

of approximately 1 µm, well-defined bimaterial spiral structures with precise alignment between the two layers of the bimaterial were realized. An overlap region of 0.5 µm between the two materials was used to enhance their adhesion. It is noteworthy that IP-Dip resin exhibits a larger change in the thermal expansion coefficient in response to the change in the laser printing power compared to IP-S. However, fabricating microjoints using IP-Dip proved to be both time consuming and less accurate, where a misalignment was observed between the two materials of the spiral, leaving IP-dip design study to future works.

The fabrication and release flowchart of the microjoint is shown in Fig. 3 (a). First, the structures were polymerized inside a drop of resin on ITO-coated soda lime glass substrates using 2PP. Then, the structures were developed in two PGMEA developer baths for 10 minutes and 2 hours, respectively, to insure the removal of all residual resin. Next, a thin aluminum layer of 600 nm was deposited by sputtering to increase the laser absorption, where aluminum is know to have high light absorption in the visible spectrum [21]. Fig. 3(b) shows a scanning electron microscope (SEM) image of the fabricated microjoint before the release process, where the components connected to the microjoint and their height (h) are also indicated. Because the fabricated microjoints were attached to the glass substrates, they needed to be released for further actuation and characterization. To achieve a successful release without damaging the microjoints, the glass substrates were first placed inside an ultrasonic bath for 10 minutes to weaken the adhesion between the structures and the substrates. Consequently, a manual micromanipulator with a thin needle were utilized to apply mechanical force to the structures for detachment. Finally, a cover glass with a double-faced adhesive tape was used to completely release the structures. The adhesive tape also created a gap between the cover glass and the microjoints to insure no friction when actuated. It is pointed out that during the release process, the microjoints often undergoes plastic deformation, which caused the connected arm to change its original orientation on the horizontal plane. Nonetheless, no noticeable effect due to plasticity was observed on the general behavior of the microjoints.

Consequently, a simple experiment was conducted to confirm the thermal response of the microjoint. In this experiment, the microjoint was placed on a hot plate (IC20 C-P, Antylia Scientific Inc., U.S.) and observed with a camera (UCMOS03100KPA, ToupCam Inc., China) mounted on a microscope. The hot plate was initially at room temperature (293 K) and its target set point was set to 353 K. The temperature increased gradually and reached the set point within approximately 450 seconds as shown in Fig. 3(c). In addition, a watch glass was placed over the hot plate to reduce the heat dissipation as much as possible. As a result, a rotational displacement of the connected arm was observed during the temperature increase as shown in Fig. 3(c), which demonstrates the response of the microjoint to the change in temperature.

B. Experimental System

An experimental system was built to confirm the characteristics of the microjoint, as shown in Fig. 4. The system mainly consists of a CMOS camera (EoSens 4CXP, Mikrotron GmbH, Germany) attached to a microscope to visualize and record the motion of the microjoint. In addition, a continuous wave (CW) laser (LAS-01087, Oxxius S.A., France) with a power of 60 mW and a wavelength of 532.1 nm was used as a laser source. Moreover, neutral-density (ND) filters were used to attenuate the laser power as needed. The laser beam was focused using an f-theta lens (S4LFT0063/121, Sill Optics GmbH & Co. KG, Germany) then reflected on a fixed right-angle mirror to strike the microjoint, where the focused laser spot size was approximately 100 µm. A notch filter (NF-25C05-40-532, Sigmakoki Inc., Japan) with a cutoff

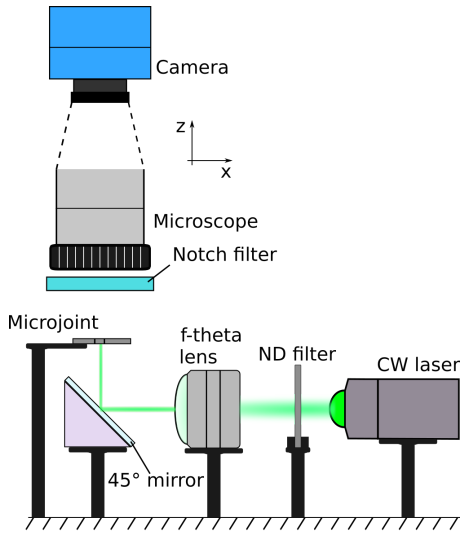

Fig. 4. Components of the experimental system for microjoint characterization.

wavelength of 532 nm was mounted before the objective of the microscope to protect the camera from the laser beam. This system configuration was used for the results presented in this article unless mentioned otherwise, where some optical components, sensors, or actuators will be added or removed as needed. Moreover, the characterization experiments were generally conducted in air environment unless mentioned otherwise.

C. Effect of Spiral Parameters

Simulations and experiments were conducted to confirm the effect of the parameters, specifically thickness and length, of the spiral on the rotational displacement and generated torque of the microjoint. In the case of thickness (c), microjoints with four different spiral thicknesses ranging from 6 µm to 18 µm with a step of 4 µm were fabricated to confirm their rotational displacement experimentally. Fig. 5(a) shows the rotational motion of a microjoint with a spiral thickness of 6 µm when hit by a laser beam with a power of approximately 8 mW (please refer to the attached video). The figure also shows the finite element analysis (FEA) of the heat induced rotational motion using COMSOL Multiphysics®. To characterize the effect of the thickness on the rotational displacement, the rotational angle $\Delta\phi$, i.e. the difference between the initial and final angles of the arm connected to the spiral, was defined as shown in Fig. 5(a). The angle was confirmed for all four different microjoints from the recorded video using offline image processing. Fig. 5(b) shows the experimental results of the rotational displacement of microjoints with different spiral thicknesses. A total of three experiments were conducted on three different microjoints for each spiral thickness and their rotational displacements were measured (red circles). The divergence in the results of different microjoints could be due to the inaccuracies in the printing process and the slight changes in the initial orientation of the arms connected to the microjoints after the release process. The results were also compared with the model defined by eq. (3), on which ΔT has been fitted, and with FEA results (black line and blue crosses respectively). It can be observed that the rotational displacement decreases with increasing thickness of the spiral, which goes in accordance with the model and the FEA. For eq. (3), the temperature increase (ΔT) and the thermal expansions coefficients (α_1, α_2) are required to compute the rotational displacement. In fact, the measurement of ΔT is challenging due to the considerably small size of the microjoint. Therefore, a least square fitting was used to minimize the error between the experimental data and the modeling data. From this, ΔT was estimated to be approximately 33.1 K, considering that $T_0 = 293.15$ K (ambient temperature), which was in the same temperature increase range compared to the results obtained using a hot plate in Section III. A. As for α_1 and α_2, the values were set to 6×10^{-5}, and 8×10^{-5} K^{-1}, respectively, according to [22]. These values were also used to compute subsequent models and FEA.

As for the effect of spiral length (L), microjoints with three different lengths were fabricated. The length of the spiral was changed by manipulating its number of turns (n). The diameter of the microjoints investigated in this experiment was increased to 160 µm to insure the elimination of unwanted material between the spiral turns when increasing their number. This increase in the diameter did not have a noticeable effect on the rotational displacement of the microjoint in case of in-air actuation due to the comparatively low thermal conductivity of air. Moreover, the fabrication of spiral microjoints with $n \geqslant 2$ proved to be quite challenging, as it was difficult to remove the residual resin between the spiral turns because of the small pitch value. Therefore, the microjoints used in this experiment had a number of turns of $n = 1, 1.25, 1.5$ corresponding to lengths $L = 588, 729, 852$ µm respectively. This length difference was sufficient to show the effect of the spiral length on the actuation of the microjoint. Fig. 5(c) shows the change of the rotational displacement against the spiral length. The red circles show the results of three repetitions conducted on three different sets of microjoints, where a linear relation can be confirmed. This also goes in accordance with the linear relation between $\Delta\phi$ and L from eq. (3) shown in the black line, and the close-to-linear relation from the FEA results shown in blue circles. However, a divergence of the experimental results compared to the model and FEA can be noticed at the first half of the figure. This could be caused by the printing inaccuracies and the release process, which can affect the parameters of the spiral.

Next, the effect of the spiral parameters on the generated torque of the microjoint was confirmed experimentally. Here, the length (L) of the spiral does not affect the torque as it can be confirmed form eq. (5) and eq. (6). Thus, only the effect of the spiral thickness (c) on

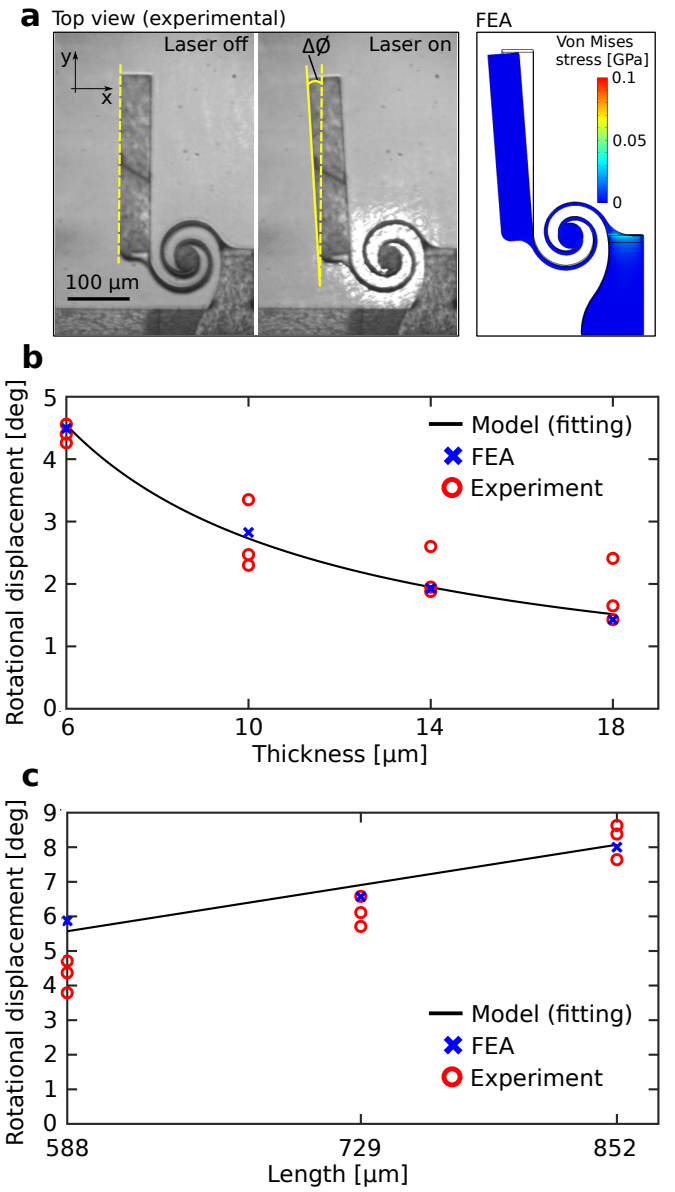

Fig. 5. Effect of spiral parameters on the rotational displacement. (a) Experimental images showing the rotational displacement ($\Delta\phi$) of the microjoint upon laser heating. The right inset shows the FEA of the heat induced rotational displacement. (b) Rotational displacement against the thickness of the microjoint. (c) Rotational displacement against the length of the microjoint. The black line, blue crosses, and red circles show the model computation (fitting), FEA, and experimental results, respectively. The red circles show the results of the three experiments conducted on three different microjoints

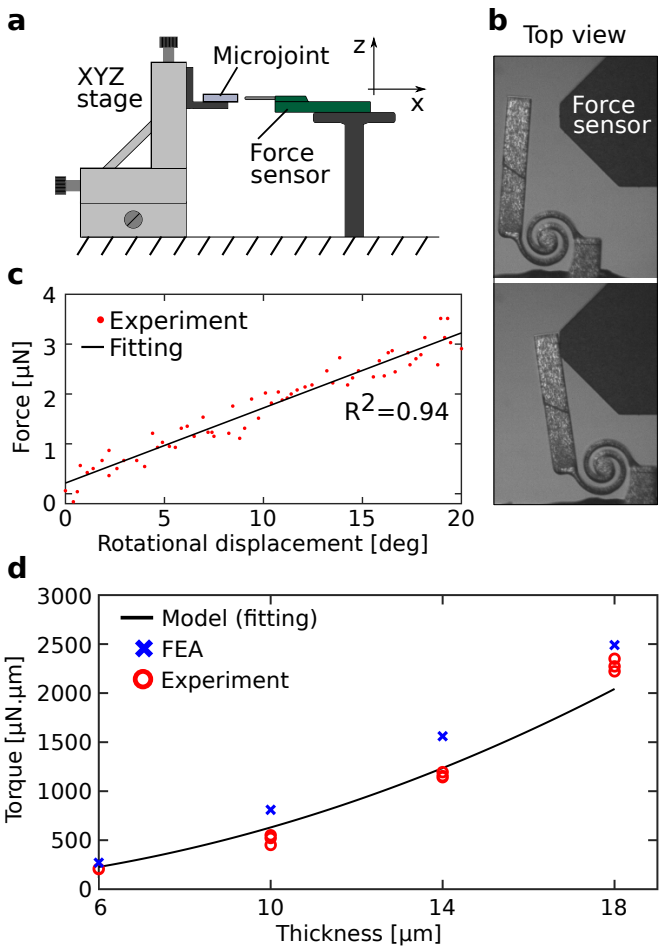

Fig. 6. Effect of spiral thickness on the generated torque. (a) The experimental setup for force measurement. (b) Experimental images showing the microjoint pushed by the force sensor. (c) Force (F) against rotational displacement ($\Delta\phi$) of the microjoint. Red circles and black line show the experimental results and the fitted curve, respectively. (d) Generated torque against the thickness of the microjoint. The black line, blue crosses, and red circles show the model computation (fitting), FEA, and experimental results, respectively. The red circles show the results of the three experiments conducted on three different microjoints

the torque was examined. The torque was measured by dividing the force at the tip of the arm connected to the microjoint by the length of this arm. In this case, a force sensor (FT-S540, Femtotools AG, Switzerland) with a range of 180 µN and a resolution of 0.05 µN was placed in front of the microjoint at the same vertical plane, as shown in Fig. 6(a). As the laser heat impacted the measurement and led to noisy results, the force characterization of the spiral microjoint was conducted while the laser was shut down. Therefore, the microjoint was placed on a manual xyz stage and moved so that the arm connected to the microjoint was pushed by the force sensor, as shown in Fig. 6(b). During the displacement, a data acquisition routine was initiated to synchronously record the sensor data (force F) and the camera images (rotational displacement $\Delta\phi$) as shown in Fig. 6(c) in red dots. A least square fitting of the measured data was conducted to get a linear relation (black line in Fig. 6(c)) with a slope (m_f). Consequently, the stiffness (k), the force (F), and the torque (τ) of the microjoint can be calculated as follows:

$$F = m_f \Delta\phi, \quad \tau = k\Delta\phi, \quad k = m_f l_{arm} \tag{7}$$

where l_{arm} is the length of the arm connected to the spiral microjoint. Fig. 6(c) demonstrates the change of the generated torque according to the spiral thickness. Similar to the case of rotational displacement, a total of three experiments were conducted on three different microjoints for each spiral thickness. Consequently, the

results of the measured torque were plotted (red circles), where it can be confirmed that the torque increases with increasing thickness of the spiral. The torques were considered at the mean experimental values of the rotational displacement demonstrated in Section III.B. In addition, the model computation of eq. (5), on which E_1, E_2 have been fitted, and the torque FEA results (black line and blue crosses, respectively) were in accordance with the experimental data. For this purpose, least square fitting was used to determine the values of the Young's modulus (E_1 = 4.6 GPa, E_2 = 1.5 GPa) to be used in eq. (5) and the FEA. These values are within the same order of magnitude compared to other works [23]. In terms of generated force, a microjoint with a 6-μm thick spiral rotated at an angle of 4.5° (its mean rotational displacement at ΔT = 33.1 K) could generate a force of approximately 0.8 μN using a 265-μm long arm.

D. In-liquid Actuation

Optothermal actuation proves to be challenging in liquid mediums due the high thermal dissipation and the localized nature of laser heating, where it is difficult to heat the whole microactuator considering a small laser spot. However, as mentioned earlier, the compactness of the spiral microjoint is a key factor allowing in-liquid actuation. The performance of the microjoint in a liquid medium was confirmed by conducting actuation experiments in water. The microjoint was placed inside a water drop as shown in the schematic of Fig. 7. For comparison, the same three sets of microjoints used in Section II. C having a diameter of 130 μm and four different thicknesses were used in this experiment. Fig. 7 shows the rotational displacement of the microjoints using two different laser powers. The blue crosses show the displacement using the same laser power (≈ 8 mW) that was used in Section II. B, here called "low laser power", where it can be confirmed that the displacement drastically decreases owing to the high thermal dissipation in water. On the other hand, the red circles show the displacement using the maximum available laser power (≈ 48 mW) by eliminating the ND filters (≈ 83% power attenuation) in the laser path, here called "high laser power". In this case, the rotational displacement is nearly equal to the case of in-air actuation demonstrating the capability of in-liquid actuation of the microjoint.

It can be observed that a variation in the displacement between in-air and in-water actuation exists. This variation is largely due to the higher heat dissipation in water compared to air, which affects the overall displacement. In addition, although the laser beam is normal to the surface and the distance it travels in water before reaching the microjoint is small (equal to the adhesive thickness of approximately 250 μm used to fix the microjoint), a small shift in the laser focal point could occur due to changes in the refraction index. Water induced reflections could also affect the total energy reaching the microjoint. A more rigorous investigation regarding the shift between in-air and in-water actuation can be addressed in future work.

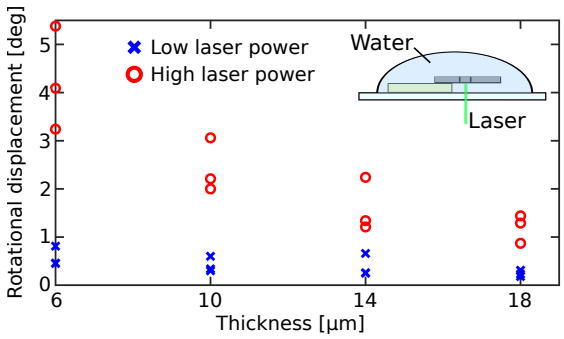

Fig. 7. In water actuation of the microjoint. Blue crosses and red circles show the rotational displacement of the microjoint using low laser power (with ND filters) and using high laser power (without ND filters), respectively. The same sets of three different microjoints were used for low and high laser powers for each thickness.

E. Repeatability, Time Response, Energy Consumption, and Proportional Actuation

The implementation of a microjoint in robotic applications favors a repeatable and fast motion that can be predicted even after multiple actuation instances. A repeatable motion that can be modeled is advantageous for further automation and control. Therefore, the repeatablity and the time response of the proposed microjoint were examined. First, to examine the repeatablity, the microjoint was actuated with a frequency of 0.5 Hz for 400 seconds. A piezoelectric tip/tilt mirror (S335, Physik Instrumente GmbH & Co. KG, Germany) was used to steer the laser beam to and away from the microjoint creating 1-second long actuation pulses. The experimental results are shown in Fig. 8(a), where it can be noticed that the rotational displacement converges exponentially with time until reaching a steady behavior. This creep behavior, i.e. an exponential convergence to a constant, is largely due to the commonly known viscoelastic nature of polymers [24]. After reaching a steady behavior, a consistent rotational displacement of the microjoint could be realized for more than 100 repetitions, which can be further confirmed from the inset of Fig. 8(a). The results demonstrate that a highly repeatable motion can be achieved by the proposed microjoint, although a time to reach a steady behavior would be required at the beginning of each use.

Next, the time response of the microjoint was confirmed from its step response, as shown in Fig. 8(b), in both air (shown in red line) and water (shown in blue line). First, the microjoint was actuated repeatedly to reach a steady behavior. Subsequently, the tip/tilt mirror was used to initiate a 1-second long laser pulse and the results were recorded by the camera using a high frame rate of 250 fps to enhance the resolution. In the case of in-air actuation using a laser power of approximately 8 mW, the time constant, i.e. the time required to reach 63% of the steady-state value after initiating or

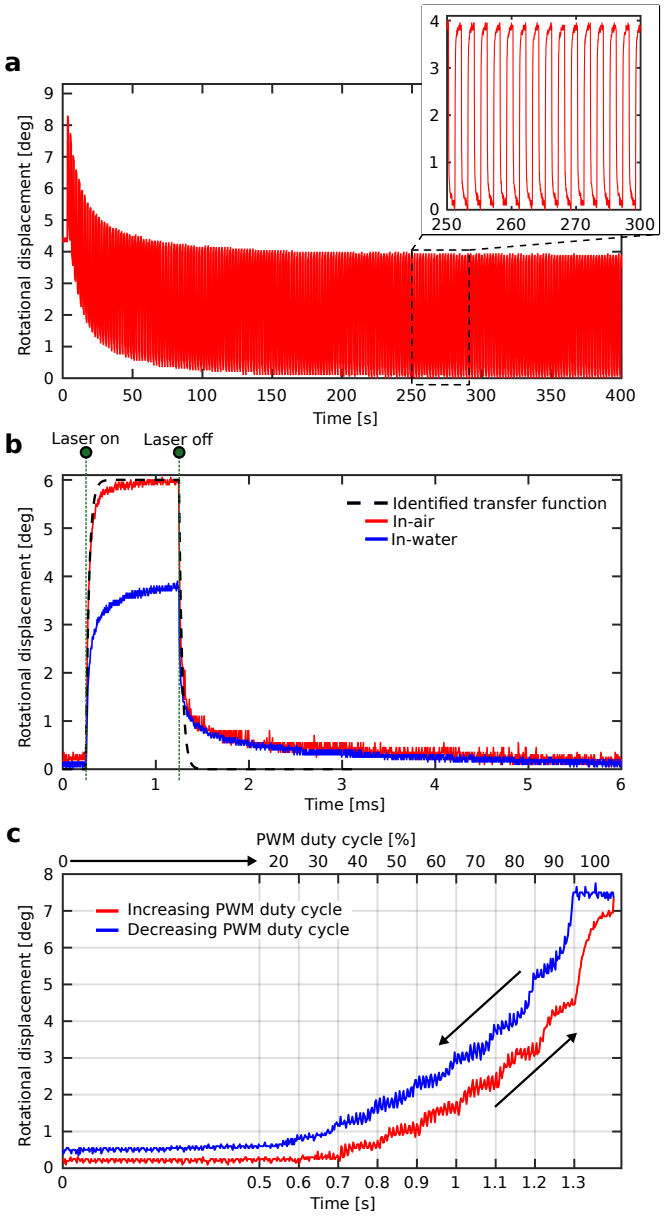

Fig. 8. Repeatability, step response, and PWM actuation. (a) Repeatability test showing the rotational displacement of the microjoint when actuated at 0.5 Hz. (b) Step response showing the rotational displacement of the microjoint when actuated by a 1-second long laser pulse. The red line, blue line, and black dashed line show in-air, in-water, and identified model step responses, respectively. (c) PWM actuation of the microjoint with a fixed frequency and a variable duty cycle. The value of each duty cycle is kept constant for 0.1 s. The red line and blue line show increasing and decreasing PWM duty cycle, respectively.

terminating the laser pulse, was approximately 34 ms for both rising and falling edges in air. In the case of in-water actuation using a laser power of approximately 48 mW, the transient section of the step response is slower. The time constant was approximately 47 ms for both the rising and falling edges of the step response in-liquid. This different time response can be due to both higher heat dissipation in-liquid, and higher viscous drag of the liquid. Nonetheless, the results demonstrate a relatively fast response of the proposed microjoint. In addition, no noticeable delay was observed between the moment of initiating the laser pulse and the starting of the rotational displacement. Consequently, by considering the microjoint as a first-order system, a transfer function could be derived from the in-air step response as follows:

$$G(s) = \frac{K_{ss} e^{-t_d s}}{t_c s + 1} = \frac{6}{0.34s + 1} \tag{8}$$

where s is the complex number of the Laplace transform, K_{ss} is the steady-state gain, t_d is the delay, and t_c is the time constant. The step response of eq. (8) is shown in Fig. 8(b) in black dashed line. It can be confirmed that the model closely matches the behavior of the actual response of the microjoint in most of the transient section. However, the final part of the transient response before reaching a steady-state value, especially in the falling edge, deviates form the actual response. This can be due to the simple first-order system used in this model. To address this issue, higher order models could be considered. Although the parameters of the transfer function can change slightly according to the used microjoint, the step response can be obtained and modeled to be used to control the microjoint in automated systems and microrobots in future works.

After obtaining the time constant of the microjoint, its energy consumption can be confirmed. For this, the laser power was measured preceding and after the microjoint using a thermal power sensor (S401C, Thorlabs Inc, U.S.) in air medium. Consequently, the consumed laser power was approximately 6.5 mW. Taking in mind the time constant of the microjoint, the energy consumption was approximately 0.221 mJ. Although this measurement does not account for power losses, such as losses caused by reflections, it serves as a good estimate of the upper band of the consumed energy.

In the context of microrobotics and microactuators, the ability to proportionally control the rotational displacement of the microjoint is advantageous. Therefore, pulse width modulation (PWM) was used to proportionally actuate microjoints to discrete positions. The PWM signal was used to drive the tip/tilt mirror to steer the laser beam with a fixed frequency of 100 Hz. The PWM duty cycle was sequentially scanned from 2 to 10 ms and then from 10 to 2 ms with increment and decrement steps of 1 ms. Each duty cycle was applied for 100 ms to have a seamless rotation of the microjoint and the rotational displacement was recorded at a frame rate of 500 fps (please refer to the attached video). Fig. 8(c) shows the change of the rotational displacement of the microjoint in response to the change in the PWM duty cycle, where a close to proportional control using PWM can be confirmed. The nonlinearity in some sections of the response is mainly due to the nonlinear behavior of the tip/tilt mirror, where the peak-to-peak positions were affected by the variable duty cycle. In this experiment, nine discrete rotational positions between 0° and 7.5° could be achieved, where more discrete positions are

TABLE I
COMPARISON BETWEEN PREVIOUS OPTOTHERMAL ACTUATORS AND THE PROPOSED MICROJOINT

Work	Design	Footprint [μm]	Displacement		Force	Response time [ms]	Medium
			Type	Value			
[12]	Bent-beam	2000 × 200	Translational	22 μm	Tens of μN order	1400	Air
[14]	Hot-cold arm	1000 × 150	Translational	3.2 μm	N.A.	40	Air and water
[15]	Bimaterial	30 × 10	Rotational	≈65°	nN order	50 ~ 100	Water
Our work	Bimaterial	160 × 160	Rotational	8.5°	μN order	34 ~ 47	Air and water

possible by increasing the duty cycle steps. In addition, hysteresis was observed in the behavior of the microjoint. This is largely due to the creep behavior cause by the viscoelastic nature of the polymer.

Table I compares the performance of the proposed microjoint to other optothermal microactuators. Our microjoint demonstrates smaller footprint, faster actuation, and versatility of the actuation medium, especially when compared to other polymer-based microactuators [12], [14]. Although hydrogel-based microactuators [15] exhibit larger rotational displacement, their generated force is approximately three orders of magnitude lower than the proposed microjoint. This is critical as higher forces are essential in micromanipulation tasks. Higher forces also allow the actuation of comparatively larger arms (similar to the arm connected to the proposed microjoint) to considerably magnify the displacement.

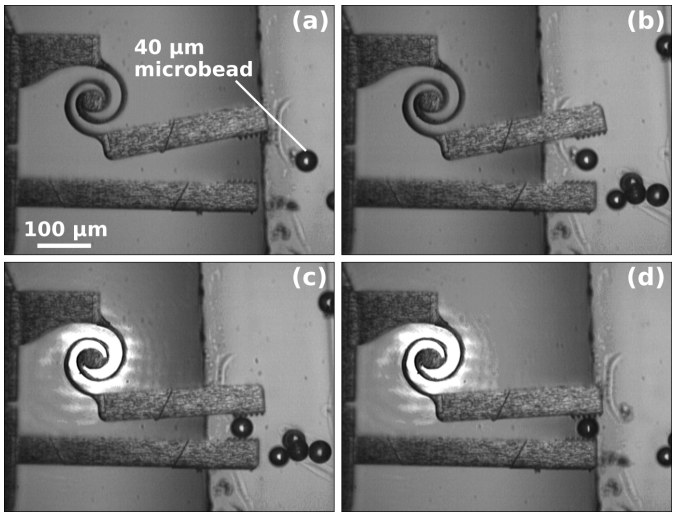

Fig. 9. Micromanipulation (Clamp-and-drag) experiment of a 40-μm diameter microbead using a microgripper incorporating the proposed microjoint as a functional element.

IV. APPLICATION TO MICROROBOTS

In this section, the proposed microjoint is implemented in two applications, a microgripper and a two-axis serial microarm, to demonstrate its practicality and performance in microrobotic applications.

A. Microgripper for Micromanipulation

Microgrippers are one of the widely used technologies to handle objects at the microscale. They are applied in many applications including biology, tissue engineering, and microassembly [25], [26]. In this experiment, a microgripper incorporating the proposed microjoint as its functional element was fabricated and used to manipulate (clamp-and-drag) a 40-μm diameter microbead. The dimensions of the microjoint were: $d = 130$ μm, $c = 6$ μm, and $n = 1$ turn. The microgripper was designed to close when actuated by the laser beam, where it should have a wide enough initial gap and a narrow enough final gap to handle the target beads. Therefore, the formerly discussed viscoelastic behaviour of the IP-S resin, which affects the steady angle of the microjoint after multiple laser actuation instances, should be taken into account when designing the microgripper. The designed microgripper had an initial gap of 20 μm in open state before being actuated. After actuating the microgripper using the laser for multiple times, the gap reached a steady value of approximately 75 μm in open state, and a gap of approximately 28 μm in closed state, which are suitable to handle the target beads.

In the experiment, the microbeads were put on a glass substrate attached to an xyz manual stage to manipulate their position, and the microgripper was attached to a stationary holder having the same vertical position as the microbeads. The stationary position of microgripper allows the microjoint to be hit by the laser for open and close motions at any instance. Fig. 9 shows snapshots of the manipulation experiment (please refer to the attached video). First, the microbead position was adjusted by the xyz stage to be between the two arms of the microgripper, which was in an open state Fig. 9(a, b). Then, the microgripper was closed by laser actuation to hold the microbead Fig. 9(c). Finally, the microbead was translated along the plane to a new position while being held by the microgripper Fig. 9(d). The advantageous remote actuation of the microjoint allows its future integration in untethered microrobots.

B. Two-axis Serial Microarm

The compactness and the selective actuation of the proposed microjoint allows the integration of multiple active joints in a microrobot. As a proof of concept, an xy serial microarm incorporating two microjoints was fabricated to demonstrate simultaneous actuation. The microjoints were connected to a link and an end

TABLE II
DISPLACEMENT OF THE MICROARM'S END EFFECTOR

Scenario	1	2	3	4
x-axis [µm]	0	31	9	14
y-axis [µm]	0	55	75	36
Overall [µm]	0	63	76	38

effector, respectively, and were perpendicular to each other, as shown in Fig. 10(a). This allows the microarm to realize relatively large displacement on both x and y-axis. The dimensions of both microjoints were: $d = 130$ µm, $c = 6$ µm, and $n = 1$ turn. In order to actuate the two microjoints with only one laser source, the tip/tilt mirror with a resolution of 1 µrad and an actuation frequency of 350 Hz was added to the experimental system.

In the experiment, four consecutive actuation scenarios were applied: both microjoints off, microjoint 1 on, microjoint 2 on, and both microjoints on. The time for each scenario was $t_1 = 2$ sec as shown in Fig. 10(b). In the case of the fourth scenario, two microjoints had to be active at the same time and the laser had to be multiplexed back and forth between the two joints in a pulsed manner. For this, the mirror was actuated at a reference frequency of 333.3 Hz (pulse duration: $t_2 = 0.003$ sec), which is 12 times shorter than the time constant of the microjoint. Fig. 10(c) shows the experimental images of the four scenarios, where the blue and cyan-colored circles indicate the position of the end effector at each scenario (please refer to the attached video). Table II shows the x-axis, y-axis, and the overall displacements of the end effector assuming that its position at scenario (1) is the center of coordinates. It can be confirmed from the figure and the table that the integration of two microjoints allows the end effector to reach positions and displacements that would not be reachable using only one microjoint, Fig. 10(c-3,4), which demonstrates the advantage of utilizing multiple active joints. Alternatively, different duty cycles of the laser, instead of a fixed one ($t_2 = 0.003$), can be used in future works to access a continuous reachable space with degrees of freedom equal to the number of microjoints.

Overall, the successful implementation of the microjoint in a microgripper and a two-axis microarm demonstrates its broad application and high potential for remotely actuated microrobotics.

V. CONCLUSION

In this article, optothermally actuated spiral rotational microjoints based on the bimaterial design for in-air and in-liquid microrobotic applications were proposed. The spiral microjoints were fabricated using 2PP to incorporate two materials with different thermal expansion coefficients and Young's modulus generating a rotational displacement upon laser heating. The microjoint was first modeled to confirm the pivotal parameters that affect its rotational displacement and generated torque.

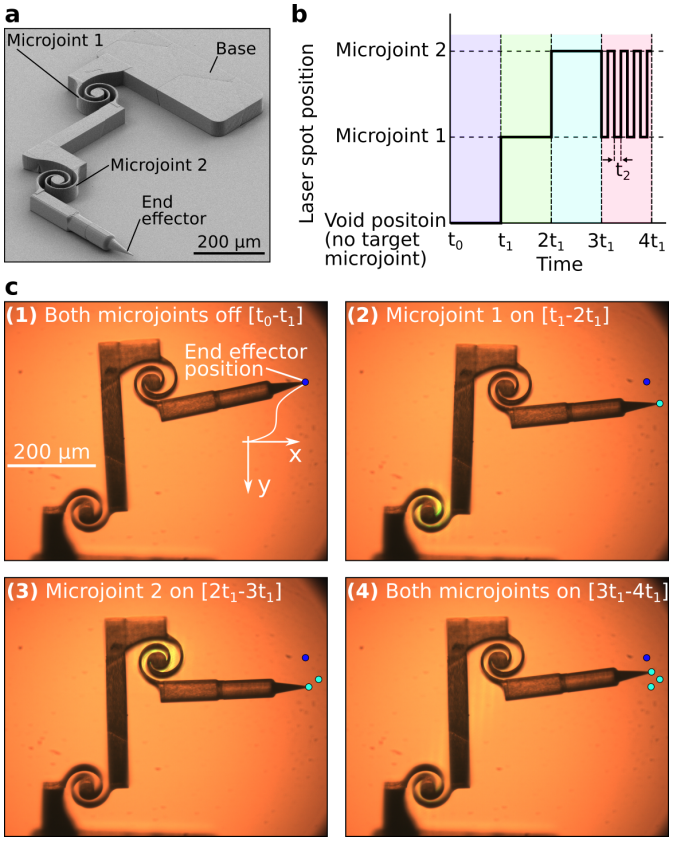

Fig. 10. Actuation of a two-axis serial microarm. (a) SEM image of the microarm incorporating two microjoints. (b) The temporal control of the laser spot position to actuate the two microjoints by using a tip/tilt mirror that was added to the experimental system, where $t_1 = 2$ sec, and $t_2 = 0.003$ sec (The time scale in the figure is adjusted for illustration purposes and does not reflect the actual scale). (c) Experimental images indicating the position of the end effector of the microarm in four consecutive actuation scenarios.

Then, microjoints with a diameter of less than 200 µm were characterized by laser actuation. The microjoints could realize a maximum rotational displacement of approximately 8.5° and a µN-order force. Moreover, a repeatable actuation of more than 100 times, a time response of approximately 36 ms, and proportional actuation were confirmed. In-liquid actuation was also confirmed by conducting experiments in water environment. Finally, the microjoints were implemented in a microgripper, where the successful manipulation of a 40-µm diameter was demonstrated, and a two-axis serial microarm, where the simultaneous actuation of multiple microjoints was shown. In future work, design optimization from geometrical and material choice aspects can be conducted to increase the rotational displacement of the microjoint [27]. In addition, we aim to utilize the spiral microjoint in a dexterous mobile microgripper for biomedical applications. This microgripper will incorporate multiple microjoints to achieve complicated motions such as rotation and release of the handled objects. Overall, the proposed microjoint showed high potential in microrobotic applications, which could open the door for highly functional and versatile microrobots.

VI. Acknowledgment

We thank Dr. Jean-Charles Beugnot at the Optics Department, FEMTO-ST Institute, France, for providing advice and equipment regarding the optical setup.

References

[1] B. V. Johnson, S. Chowdhury, and D. J. Cappelleri, "Local magnetic field design and characterization for independent closed-loop control of multiple mobile microrobots," *IEEE/ASME Transactions on Mechatronics*, vol. 25, no. 2, pp. 526–534, 2020.

[2] B. Ahmad, M. Gauthier, G. J. Laurent, and A. Bolopion, "Mobile microrobots for in vitro biomedical applications: A survey," *IEEE Transactions on Robotics*, 2021.

[3] Z. Yang, L. Yang, and L. Zhang, "Autonomous navigation of magnetic microrobots in a large workspace using mobile-coil system," *IEEE/ASME Transactions on Mechatronics*, 2021.

[4] B. M. Bhushan, J. Y. Yoon, L. G. Griffith, and D. L. Trumper, "Flux-biased, energy-efficient electromagnetic micropumps utilizing bistable magnetic latching and energy storage springs," *IEEE/ASME Transactions on Mechatronics*, 2020.

[5] R. Sriramshankar and G. Jayanth, "An integrated magnetic actuation system for high-speed atomic force microscopy," *IEEE/ASME Transactions on Mechatronics*, vol. 23, no. 5, pp. 2285–2294, 2018.

[6] Q. Chen, P. Lv, T.-Y. Huang, J. Huang, and H. Duan, "Encoding smart microjoints for microcrawlers with enhanced locomotion," *Advanced Intelligent Systems*, vol. 2, no. 3, p. 1900128, 2020.

[7] H. Shigemune, S. Maeda, Y. Hara, N. Hosoya, and S. Hashimoto, "Origami robot: a self-folding paper robot with an electrothermal actuator created by printing," *IEEE/ASME Transactions On Mechatronics*, vol. 21, no. 6, pp. 2746–2754, 2016.

[8] J. Zhang, D. Torres, J. L. Ebel, N. Sepúlveda, and X. Tan, "A composite hysteresis model in self-sensing feedback control of fully integrated VO_2 microactuators," *IEEE/ASME Transactions on Mechatronics*, vol. 21, no. 5, pp. 2405–2417, 2016.

[9] J. H. Jung, C. Han, S. A. Lee, J. Kim, and C. Yang, "Microfluidic-integrated laser-controlled microactuators with on-chip microscopy imaging functionality," *Lab on a Chip*, vol. 14, no. 19, pp. 3781–3789, 2014.

[10] D.-S. Chen, P.-F. Yeh, Y.-f. Chen, C.-W. Tsai, C.-Y. Yin, R.-J. Lai, and J.-c. Tsai, "An electrothermal actuator with two degrees of freedom serving as the arm of a mems gripper," *IEEE Transactions on Industrial Electronics*, vol. 61, no. 10, pp. 5465–5471, 2014.

[11] M. Sitti and D. S. Wiersma, "Pros and cons: Magnetic versus optical microrobots," *Advanced Materials*, vol. 32, no. 20, p. 1906766, 2020.

[12] C. Elbuken, M. B. Khamesee, and M. Yavuz, "Design and implementation of a micromanipulation system using a magnetically levitated mems robot," *IEEE/ASME Transactions on Mechatronics*, vol. 14, no. 4, pp. 434–445, 2009.

[13] R. Zhang, A. Sherehiy, Z. Yang, D. Wei, C. K. Harnett, and D. O. Popa, "Chevbot–an untethered microrobot powered by laser for microfactory applications," in *IEEE International Conference on Robotics and Automation (ICRA)*, pp. 231–236, 2019.

[14] Q. You, Y. Wang, Z. Zhang, H. Zhang, T. Tsuchiya, and O. Tabata, "Laser-driven optothermal microactuator operated in water," *Applied Optics*, vol. 59, no. 6, pp. 1627–1632, 2020.

[15] M. Hippler, E. Blasco, J. Qu, M. Tanaka, C. Barner-Kowollik, M. Wegener, and M. Bastmeyer, "Controlling the shape of 3d microstructures by temperature and light," *Nature Communications*, vol. 10, no. 1, pp. 1–8, 2019.

[16] Y. Zhou, A. W. Hauser, N. P. Bende, M. G. Kuzyk, and R. C. Hayward, "Waveguiding microactuators based on a photothermally responsive nanocomposite hydrogel," *Advanced Functional Materials*, vol. 26, no. 30, pp. 5447–5452, 2016.

[17] J. Li, Q. Ma, Y. Xu, M. Yang, Q. Wu, F. Wang, and P. Sun, "Highly bidirectional bendable actuator engineered by lcst–ucst bilayer hydrogel with enhanced interface," *ACS Applied Materials & Interfaces*, vol. 12, no. 49, pp. 55290–55298, 2020.

[18] A. Dochshanov, M. Verotti, and N. P. Belfiore, "A comprehensive survey on microgrippers design: Operational strategy," *Journal of Mechanical Design*, vol. 139, no. 7, 2017.

[19] P. Khadkikar, "The principles and properties of thermostat metals," *JOM*, vol. 45, no. 6, pp. 39–42, 1993.

[20] *Kanthal Thermostatic Bimetal Handbook*. 6th ed., Kanthal AB Co., Hallstahammar, Sweden, 2008.

[21] S. S. Mirshafieyan and J. Guo, "Silicon colors: spectral selective perfect light absorption in single layer silicon films on aluminum surface and its thermal tunability," *Optics Express*, vol. 22, no. 25, pp. 31545–31554, 2014.

[22] W. Huang and K. M. de Payrebrune, "Experimental investigation on the thermal length expansion of direct laser writing material," *PAMM*, vol. 19, no. 1, p. e201900485, 2019.

[23] Y. Liu, O. Stein, J. H. Campbell, L. Jiang, N. Petta, and Y. Lu, "Three-dimensional printing and deformation behavior of low-density target structures by two-photon polymerization," in *Nanoengineering: Fabrication, Properties, Optics, and Devices XIV*, vol. 10354, p. 103541U, International Society for Optics and Photonics, 2017.

[24] N. Rohbeck, R. Ramachandramoorthy, D. Casari, P. Schürch, T. E. Edwards, L. Schilinsky, L. Philippe, J. Schwiedrzik, and J. Michler, "Effect of high strain rates and temperature on the micromechanical properties of 3d-printed polymer structures made by two-photon lithography," *Materials & Design*, vol. 195, p. 108977, 2020.

[25] C. Shi, X. Dong, and Z. Yang, "A microgripper with a large magnification ratio and high structural stiffness based on a flexure-enabled mechanism," *IEEE/ASME Transactions on Mechatronics*, 2021.

[26] D. Liu, X. Liu, P. Li, X. Tang, M. Kojima, Q. Huang, and T. Arai, "All-purpose magnetic micromanipulation system with two modes: Chopstick-like two-finger microhand and hydrodynamic tweezer," *IEEE/ASME Transactions on Mechatronics*, 2021.

[27] Y. Wang, M. Li, J.-K. Chang, D. Aurelio, W. Li, B. J. Kim, J. H. Kim, M. Liscidini, J. A. Rogers, and F. G. Omenetto, "Light-activated shape morphing and light-tracking materials using biopolymer-based programmable photonic nanostructures," *Nature communications*, vol. 12, no. 1, pp. 1–9, 2021.

Belal Ahmad received his MSc and Ph.D. in engineering from Kyushu Institute of Technology, Kitakyushu, Japan, in 2015 and 2019, respectively. He is currently a postdoctoral researcher at the Automatic Control and Micro-Mechatronic Systems Department, FEMTO-ST, Besancon, France. His main research interests are microrobotics, robotic systems integration, and high-speed tracking.

Antoine Barbot received a Ph.D in 2016 C2N-CNRS in Paris. He then started a postdoctoral position at Imperial College London where he focused on microrobotics applied to non-invasive surgery. He particularly developed floating magnetic microrobots for flexible microelectronic assembly as well as micropneumatic and microfluidic actuators embedded at a capillary tip. Since 2020, he is CNRS researcher at FEMTO-ST institute in Besançon, France. He focuses on capillary force for microrobotics.

Gwenn Ulliac received his Ph.D degree in Micro-technologies in 2005 from the University of Lille 1, Lille, France in collaboration with Thales Airborne Systems. He is currently a Research Engineer at the FEMTO-ST Institute, Besançon, France. He works in the field of micro-nanofabrication in clean-room and more particularly of 3D objects by using two-photon polymerization technology.

Aude Bolopion received her Ph.D. degree in robotics in 2010 from Sorbonne University (ex. Pierre et Marie Curie University), Paris, France. She was a member of the ISIR Institute. Her research interests are focused on microrobotics and micromanipulation. She got a CNRS researcher permanent position at the FEMTO-ST Institute, Besancon, France in 2011. She received the CNRS bronze medal in 2019 for her work on non contact actuation for microrobotics.